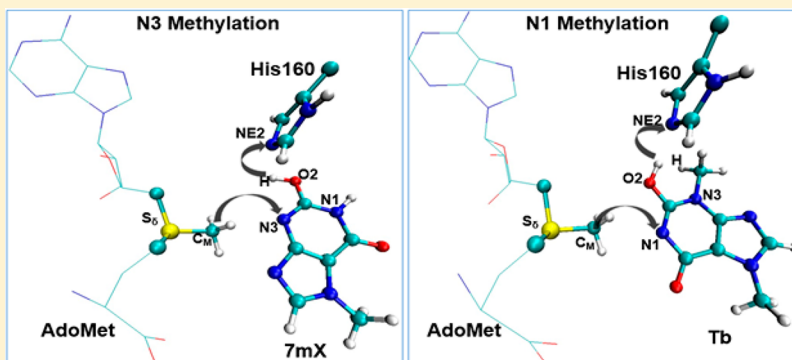


Quantum Mechanical/Molecular Mechanical Study of Catalytic Mechanism and Role of Key Residues in Methylation Reactions Catalyzed by Dimethylxanthine Methyltransferase in Caffeine Biosynthesis

Yufei Yue and Hong Guo*

Department of Biochemistry and Cellular and Molecular Biology, University of Tennessee, Knoxville, Tennessee 37996, United States

Supporting Information



ABSTRACT: The caffeine biosynthetic pathway is of considerable importance for the beverage and pharmaceutical industries which produces two blockbuster products: theobromine and caffeine. The major biochemistry in caffeine biosynthesis starts from the initial substrate of xanthosine and ends with the final product caffeine, with theobromine serving as an intermediate. The key enzyme, S-adenosyl-L-methionine (SAM) dependent 3,7-dimethyl-xanthine methyltransferase (DXMT), catalyzes two important methyl transfer steps in caffeine biosynthesis: (1) methylation of N3 of 7-methylxanthine (7mX) to form theobromine (Tb); (2) methylation of N1 of theobromine to form caffeine (Cf). Although DXMT has been structurally characterized recently, our understanding of the detailed catalytic mechanism and role of key catalytic residues is still lacking. In this work, the quantum mechanical/molecular mechanical (QM/MM) MD and free energy simulations are performed to elucidate the catalytic mechanism of the enzyme-catalyzed reactions and to explain experimental observations concerning the activity of this enzyme. The roles of certain active-site residues are studied, and the results of computer simulation seem to suggest that a histidine residue (His160) at the active site of DXMT may act as a general base/acid catalyst during the methyl transfer process.

INTRODUCTION

As one of the best known plant alkaloids, caffeine (1,3,7-trimethylxanthine) is produced in seeds, leaves, and fruits of many higher plants, including three very important crops: coffee (*Coffea arabica* and *Coffea canephora*), cacao (*Theobroma cacao*), and tea (*Camellia sinensis*).¹ It is a secondary metabolite in plants and can work as a native insect repellent² and inhibitor to germination of other seeds.³ However, it is probably better known as a human central nervous system stimulant, widely used in the beverage and pharmaceutical industries. The main pathway of caffeine biosynthesis starts from the initial substrate xanthosine (XR) and ends with the final product of caffeine, involving three S-adenosyl-L-methionine (SAM) dependent N-methyl transfer processes and one ribose removal step (Figure 1).¹ In this biosynthetic pathway, the ribose is removed and 7-N, 3-N, and 1-N on the purine alkaloid are methylated (Figure 1), producing 7-methylxanthosine (7mXR), 7-methylxanthine

(7mX), and theobromine (3,7-dimethylxanthine, Tb) as intermediates.

Eleven enzymes that participate in this pathway have been isolated so far and identified as *N*-methyltransferase.^{4–9} These enzymes catalyze the *N*-methylation of nitrogen-containing compounds and belong to the wider motif B' methyltransferase family, which is plant specific and catalyzes SAM-dependent substrate methylation.¹⁰ Only two of these enzymes in the pathway, xanthosine methyltransferases (XMT), and 3,7-dimethylxanthine methyltransferase (DXMT), both from *Coffea canephora* “robusta”, have been structurally characterized.¹¹ XMT is capable of catalyzing the methyl transfer to XR and, probably, the nucleotide cleavage of XR as well.¹¹ DXMT has dual activities toward both 7mX(3-N) and Tb(1-N).¹¹

Received: October 30, 2013

Published: January 17, 2014



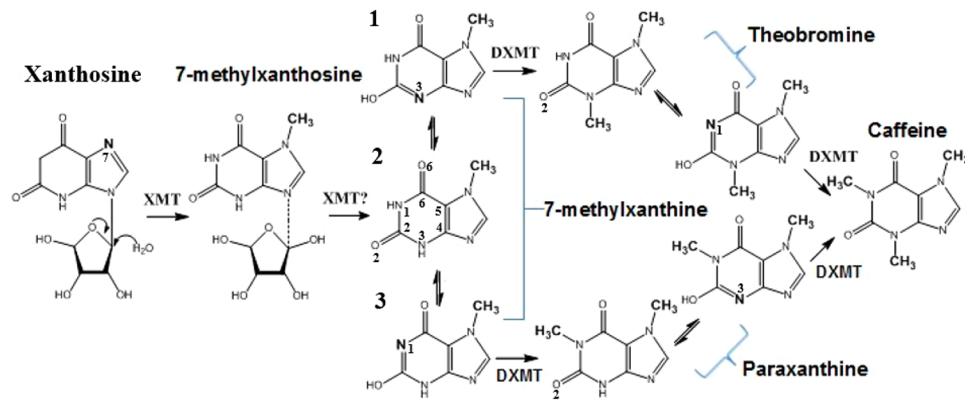


Figure 1. Caffeine biosynthesis pathway in *Coffea canephora* "robusta". The conversion of xanthosine to caffeine involves three N-methylation steps and the removal of a ribose moiety. The major pathway is through an intermediate product, theobromine. However, the pathway through the intermediate paraxanthine is also potentially possible. The nitrogen atoms undergoing methylation, and transferred methyl groups are highlighted in bold. Note 7-methylxanthine, theobromine, and paraxanthine may exist as different tautomers. Three of the tautomers (1, 2, and 3) for 7-methylxanthine are shown in this figure. The tautomer with the hydroxyl at C6 is not considered here, because there seems no potential general base/acid catalyst for the methyl transfer in the X-ray structure (see below). Tautomers 1 and 3 can undergo N3 and N1 methylation, respectively.

Previous experimental studies have indicated that substrate recognition and catalytic efficiency of DXMT and other members of the family appear to have subtle biochemical characteristics, and their dependences on the active site and other residues may be complicated.^{9,11,12} Therefore, it is of considerable interest to determine the subtle structure features in the active site that control the substrate recognition and catalytic efficiency of DXMT. Moreover, a detailed study of the substrate specificity for DXMT could help to identify the key residues in the active site that might be genetically modified by site-directed mutagenesis to generate, for instance, decaffeinated coffee species. The overall structure of DXMT was found to resemble that of salicylic acid O-methyltransferase, SAMT,¹¹ which is another SAM-dependent motif B' methyltransferase that has been structurally identified.¹³ Yao et al. performed computer simulations on the methyl transfer catalyzed by SAMT (from SAM to salicylic acid) by using hybrid quantum mechanical and molecular mechanical (QM/MM) molecular dynamic (MD) simulations.¹⁴ They suggested based on the results of computer simulations that the computational approaches seem to be well suited for the investigations of enzyme-catalyzed methyl transfer processes.^{15–17}

Although the X-ray structure of DXMT has been determined, the catalytic mechanism of the enzyme is still not clear. For instance, Figure 1 shows that a general base seems to be required to remove the proton of the hydroxyl group (e.g., at the 2 position) in order to have the methyl group transferred to the nitrogen (e.g., either the 3 or 1 position) in each case. However, the general base or general bases have not been clearly identified so far. In this work, QM/MM MD and free energy simulations are performed to determine the catalytic mechanism of the enzyme-catalyzed reactions involving DXMT and to explain some experimental observations. The results of the simulations seem to suggest that a conserved residue, His160, may act as a general base/acid catalyst for the conversion of 7-methylxanthine to caffeine with theobromine as an intermediate product.

METHODS

The initial coordinates for the reactant complex of the methyl transfer to N3 or N1 of the purine ring are based on the crystallographic complex (PDB ID: 2EFJ) of DXMT containing

AdoHcy and theobromine with two different orientations. The QM/MM MD and free energy (potential of mean force, PMF) simulations were performed in the determination of free energy profiles for the methylation processes with the CHARMM program.¹⁸ Water spheres based on a modified TIP3P water model¹⁹ with radius of 30 Å and centered at either N3 or N1 of the purine ring were used to solvate the systems. A stochastic boundary with a Poisson–Boltzmann charge-scaling scheme²⁰ was applied. The reservoir region has $r > 22$ Å, and the buffer region has radius (r) equal to $20 \leq r \leq 22$ Å. The reaction region has $r \leq 20$ Å. The methyl donating AdoMet, the substrate (7mX or Tb), and the side chain of His160 were treated by QM, and the rest of the system by MM. An all-hydrogen potential function (PARAM27)²¹ was used for the MM region, and the self-consistence charge density functional tight binding (SCC-DFTB)^{22,23} method was used for the QM region. The link-atom approach²⁴ was used to separate the QM and MM regions. A small system containing the side chain of His160, a part of AdoMet, and the complete 7mX molecule was studied by using the SCC-DFTB method with partial energy minimization and high level MP2/6-31G** single-point calculations to determine the accuracy of the SCC-DFTB method. The results seem to suggest that the SCC-DFTB method should perform reasonably well for the systems (Figure S1, see the Supporting Information).

To build the initial reactant complex for the N3 methylation on 7mX from the X-ray structure, the product analog was modified to 7mX by deleting the methyl group at its N3 position and a methyl group was added to S_{δ} of AdoHcy to generate the methyl-donor AdoMet. Similarly, to build the initial reactant complex for the N1 methylation on Tb, AdoHcy was modified to AdoMet by adding a methyl group. The initial reactant complex for the N1 methylation on 7mX was built by deleting the methyl group on N3 of the original Tb substrate in the crystal structure. The initial reactant complex containing paraxanthine (Px) was generated by adding a methyl group to N1 and deleting a methyl group on N3 of Tb in the crystal structure. The reference center for partitioning the system was chosen to be either N3 or N1 of the substrate, depending on which atom is the methyl acceptor. The resulting systems contain about 5800 atoms, including about 600 water molecules. The initial structures for the entire stochastic

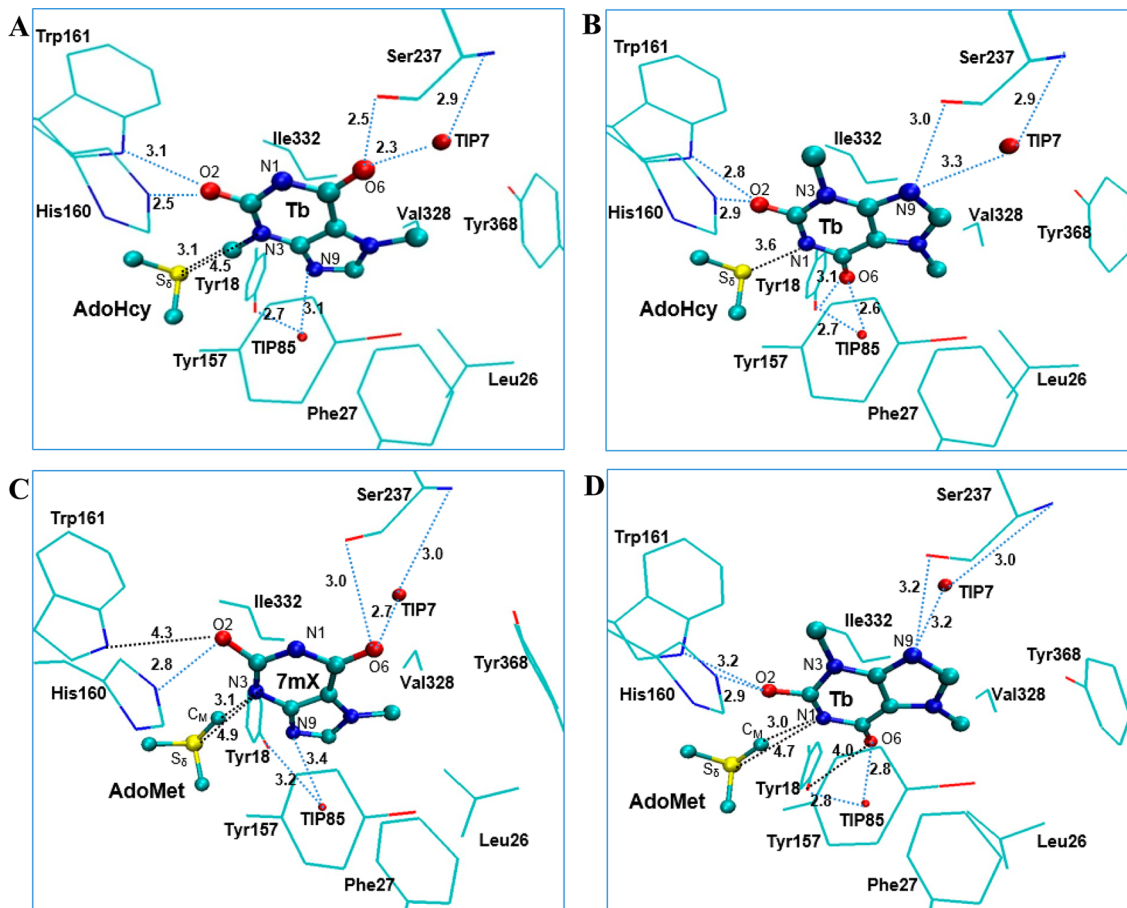


Figure 2. (A) Active site in the X-ray structure of DXMT (PDB ID: 2EFJ) complexed with AdoHcy and Tb. DXMT is shown in sticks, and AdoHcy and Tb are in balls and sticks. Only the three atoms, C5', CG, and S_δ, from AdoHcy and the residues that are close to Tb are shown for clarity. Possible hydrogen bonds are shown in blue dotted lines. Some distances are given with units of angstroms. (B) Active site in the X-ray structure of DXMT complexed with AdoHcy and Tb with different orientation. (C) Average active-site structure of the reactant complex containing AdoMet and 7mX from simulations. (D) Average active-site structure of the reactant complex containing AdoMet and Tb from simulations.

boundary systems were optimized using the steepest descent (SD) and adopted-basis Newton–Raphson (ABNR) methods. The systems were gradually heated from 50.0 to 298.15 K in 50 ps. A 1-fs time step was applied for the integration of equation of motion, and the coordinates were saved every 50 fs. Initially, 1.5 ns QM/MM MD simulations were executed for each of the reactant complexes. Similar to the methyl transfer from AdoMet to salicylic acid catalyzed by SAMT,¹⁴ the S_N2 methyl transfer reaction from AdoMet to N(1/3) on the DXMT's substrate is presumably more efficient if the S_δ-CH₃ group of AdoMet is well aligned with the lone pair of electrons of N(1/3) in the reactant complexes. The reaction coordinate was defined as a linear combination of $r(C_{\text{M}} \cdots N_{1/3})$ and $r(S_{\delta} \cdots C_{\text{M}})$, which is $R = r(S_{\delta} \cdots C_{\text{M}}) - r(C_{\text{M}} \cdots N_{1/3})$. The umbrella sampling method²⁵ implemented in the CHARMM program along with the Weighted Histogram Analysis Method (WHAM)²⁶ was applied to determine the free energy (PMF) as a function of the reaction coordinate(s) for the methyl transfer process. For each methyl transfer process, twenty simulation windows were saved, and for each window 50 ps production runs were performed after 50 ps equilibration. The force constants of the harmonic biasing potentials used in the PMF simulations were 50–500 kcal mol⁻¹ Å⁻². The simulations were also performed with the O–H bond on the substrate fixed by SHAKE²⁷ algorithm of CHARMM. The SHAKE algorithm was used here to avoid proton transfer from the substrate to the NE2 position of

His160 and to estimate the effect of the proton transfer on the methyl transfer.

The 2D free energy map (PMF) for the conversion of 7mX to Tb was also determined with the umbrella sampling method²⁵ and two-dimensional WHAM.²⁶ The time step for QM/MM MD simulation is 1 fs. One reaction coordinate is $R_x = r(S_{\delta} \cdots C_{\text{M}}) - r(C_{\text{M}} \cdots N_3)$, describing the methyl transfer process. The other reaction coordinate is the distance between H on the hydroxyl group of 7mX and NE2 on His160, $R_y = r(H \cdots \text{NE2})$, describing the proton transfer process. 209 windows were used in the calculation of 2D PMF, and 50 ps production runs were preformed after 50 ps equilibration for each window. The force constants for each window were in the range of 100–400 kcal mol⁻¹ Å⁻² for both R_x and R_y .

RESULTS AND DISCUSSIONS

Reactant Complexes for N3 and N1 Methylation. The X-ray structures of the DXMT complexes have been available.¹¹ As is shown in Figure 2A, Tb has its N3 methyl group pointing to S_δ of AdoHcy in one orientation in the X-ray structure. This is in contrast with the case of another orientation of Tb in the X-ray structure in which N1 of Tb (instead of N3) is close to S_δ (Figure 2B). Both of these orientations are presumably stabilized in the active site by hydrogen binding interactions, including the interactions of O2 of Tb with the side chains of

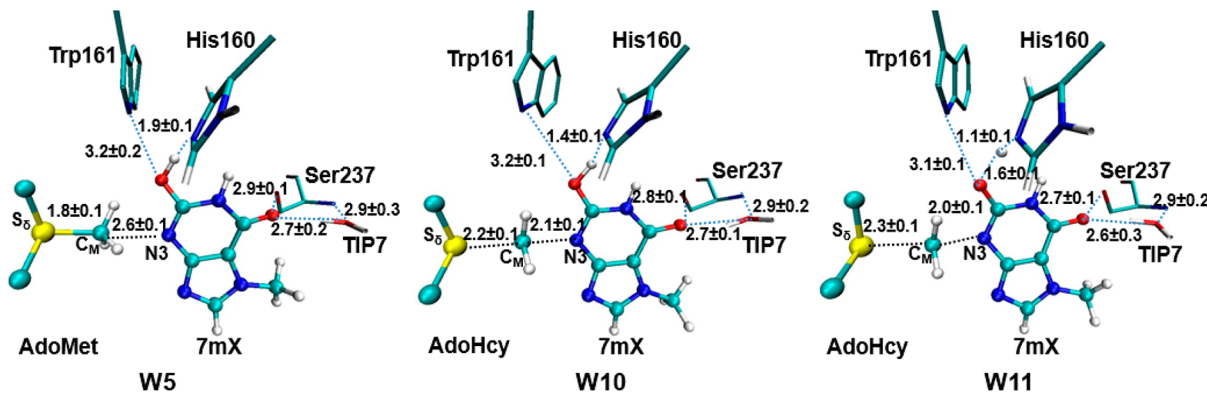


Figure 3. Active-site structure during the free energy simulation of N3 methylation ($7mX \rightarrow Tb$). The average structures in window 5 (W5, before reaching the transition state, TS), window 10 (W10, near TS), and window 11 (W11, passed TS) of N3 methylation are shown. The possible hydrogen bonding between $7mX$ and nearby residues are shown in blue dotted lines. Some average distances are given with units of angstrom.

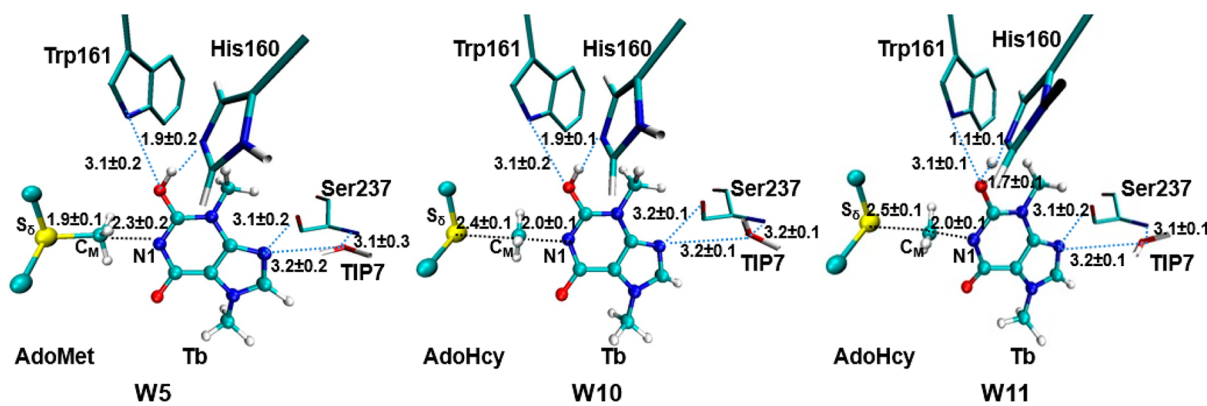


Figure 4. Active-site structure during the free energy simulation of N1 methylation ($Tb \rightarrow Cf$). The average structures in window 5 (W5, before reaching TS), window 10 (W10, near TS), and window 11 (W11, passed TS) of N1 methylation are shown. The possible hydrogen bonding between Tb and nearby residues are shown in blue dotted lines. Some average distances are given with the unit of angstrom.

His160 and Trp161 as well as the hydrogen bond involving the hydroxyl group of Ser237 and O6 in Figure 2A (N9 in Figure 2B). Moreover, water mediated hydrogen bonds are also formed involving the backbone N–H group of Ser237 and O6 in Figure 2A (or N9 in Figure 2B) and the hydroxyl group of Tyr18 and N9 in Figure 2A (Try18 and O6 in Figure 2B). As is evident from Figure 2A and B, there is no potential general base/acid catalyst near O6. In addition to the hydrogen bonding interactions, the existence of hydrophobic environment can also be seen in Figure 2A and B. For instance, the purine ring forms hydrophobic contacts with Ile332 and Tyr157, while Phe27, Leu26, Tyr368, and Val328 produce a hydrophobic core. These hydrophobic interactions may also make contributions to the binding.

The average structures of the reactant complexes for the conversions of $7mX$ to Tb and Tb to Cf obtained from 1 ns QM/MM MD simulations are shown in Figure 2C and D, respectively. The hydrogen bonding and hydrophobic interactions discussed earlier for the original crystal structures (Figure 2A and B) generally remain (see Figure 2C and D). However, there are some deviations. This can be seen by comparison of Figure 2A with C and Figure 2B with D, respectively. These differences might be explained in part by the fact that, unlike the crystal structure, the reactant complex contains AdoMet rather than AdoHcy. The existence of a positively charged methyl group on AdoMet is expected to produce some changes in the interactions, leading to

modifications of the active-site structure. For instance, the distance from S_δ to N1 increased from 3.6 Å in Figure 2B to 4.7 Å in Figure 2D. For the reactant complexes of other methyltransferases including PKMT,^{15,31–33} PRMT,³⁴ and SAMT,¹⁴ the methyl transfer processes appear to be favorable if the distance between the methyl group from methyl donor and acceptor nitrogen (or oxygen) is around 3 Å. This seems to be the case for the systems studied here, as can be seen from Figure 2C and D. Figure 2C and D also show that the methyl group of AdoMet is well aligned with the lone-pair electrons of N3 from $7mX$ and N1 from Tb, respectively, in the reactant complexes. It has been indicated from previous studies on SAMT¹⁴ and PKMTs^{15–17} that a good alignment between the transferable methyl group and the lone pair of electrons of its acceptor, such as nitrogen and oxygen, is of importance for an efficient methyl transfer. The simulation results reported here suggest that the DMXT reactant complex containing either $7mX$ or Tb in the active site could meet the requirement for a good alignment of the reactive groups participating in the methyl transfer, consistent with the substrate specificity^{9,11} of this enzyme. As discussed below, the free energy simulations from the reactant complex to transition state indicates that a proper balance of hydrogen bonding and hydrophobic interactions appears to be responsible for the good alignment of the reactive groups in the methyl transfer process.

His160 as General Acid/Base Catalyst for N3 and N1 Methylation. $7mX$ may exist in one of the tautomers in

solution (see Figure 1).²⁸ Methyl transfer from AdoMet to N3 on 7mX is presumably an S_N2 reaction in which the lone pair of electrons from the nucleophile N3 attacks C_M of the methyl group. Although the normal pK_a of histidine imidazole in solution is around 6, different prediction methods seem to indicate that His160 in the active site of DXMT may have a lower pK_a (3.21 by ProPka;²⁹ <0 by H++³⁰). Therefore, His160 may be neutral at around pH 7–9 when the enzyme is active, making it more likely to act as a general base. The neighboring O2 of 7mX and the side chain of Tyr157 might contribute to lowering the pK_a of imidazole of His160.²⁹ In the crystal structure, the atom NE2 of His160 is within 2.5 Å of the atom O2 on the substrate (Figure 2A). After 1 ns MD simulation, the distance between NE2 and O2 is slightly increased to be 2.8 Å (Figure 2C). Thus, it is likely that NE2 on His160 might help to stabilize the hydroxyl O2 on 7mX through strong hydrogen bonding in the reactant complex and act as the general base during the methyl transfer. Tb also has different tautomers, with either deprotonated N1 or deprotonated O2 (Figure 1). After 1 ns MD simulation, NE2 of His160 is well kept at 2.9 Å to O2 of the substrate (Figure 2B), the same as in the crystal structure (Figure 2D). It is thus likely that, similar to the case involving 7mX, NE2 on His160 might help to stabilize the hydroxyl O2 on Tb through strong hydrogen bonding and act as a general base as well. Consistent with the suggestion above, the distance between Trp161 and O2 are reasonably maintained during the simulations (see Figure 3 and 4), possibly contributing as another stabilizing force of O2 on the substrate.

The hydrophobic interactions in all the simulations (see Figures 3 and 4) remain basically the same as those observed in the X-ray structure; for clarity, they are not shown in Figures 3 and 4. It is of interest to note that the active-site water molecule, TIP85, moves away from the active site (see Figure 2). Nevertheless, the distance between the nitrogen on the side chain of Trp161 and O2 of substrate is well kept at round 3.2 Å as shown in Figures 3 and 4. The hydrogen bond between Trp161 and the hydroxyl O2 on the substrate appears to help to maintain the substrate in the reactive configuration for the methyl transfer. The hydrogen bonding interactions of the backbone nitrogen from Ser237 with either O6 of 7mX or N9 of Tb as well as those mediated by the water molecule are generally stable in all simulations; they may play an important role in generating the reactive configuration for the reactant complex as well.

The role of His160 as a general base is further demonstrated in the free energy simulations of methyl transfer processes. As is shown in Figures 3 or 4, a spontaneous proton transfer from O2 to neutral His160 occurred during methylation of N3 (7mX → Tb) or N1 (Tb → Cf). In Figure 3, the structure in window 10 shows that the average distance between the proton and NE2 of His160 is 1.4 Å, while that in window 11 shows that the proton transfer has basically completed (H···NE2 average distance is 1.1 Å). In Figure 4, the structure in window 10 shows that the average distance between the proton and NE2 of His160 is 1.9 Å, while that in window 11 shows that the proton transfer has basically completed (H···NE2 average distance is 1.1 Å).

To monitor the breakage of O–H bond of the substrate and the formation of N–H bond between H and NE2 of His160, the distance between H and NE2 as a function of the reaction coordinate, $R = r(S_\delta \cdots C_M) - r(C_M \cdots N_{1/3})$, was plotted in Figure 5. The N–H covalent bond is considered being formed

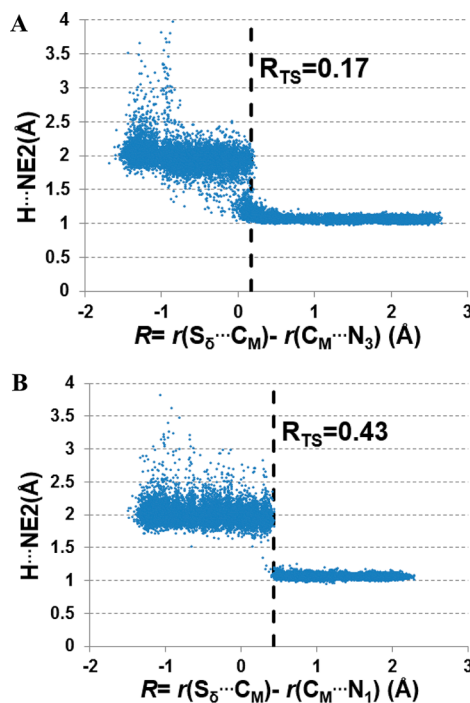


Figure 5. Distance between H on the substrate and NE2 on His160 as a function of the reaction coordinate. (A) Methylation of N₃ (7mX → Tb). (B) Methylation of N₁ (Tb → Cf). Note that O–H is broken and N–H is formed when the distance between H and NE2 is about 1.1 Å. The reaction coordinate for the transition is shown as R_{TS} in a dotted line.

when the distance between H and NE2 is less than 1.1 Å. Figure 5A and B shows that the N–H bond is formed near $R = 0.17$ Å for N₃ methylation and $R = 0.43$ Å for N₁ methylation. Furthermore, they show that the proton transfer and the breakage of S_δ–C_M bond are not concerted, which is consistent with the two-dimensional free energy map (see Figure 7 below).

Free Energy Profiles of Methyl Transfer Processes.

The free energy profiles (potential of mean force) for the methyl transfer from AdoMet to 7mX and Tb are plotted in Figure 6A and B, respectively, as a function of the reaction coordinate ($R = r(S_\delta \cdots C_M) - r(C_M \cdots N_3)$ in Figure 6A and $R = r(S_\delta \cdots C_M) - r(C_M \cdots N_1)$ in Figure 6B). As can be seen from Figure 6A, the free energy barrier from the initial reactant complex to the transition state is calculated to be about 16–17 kcal/mol for the first methyl transfer to 7mX. And this free energy barrier is estimated to be about 18 kcal/mol for the second methyl transfer to Tb as shown in Figure 6B. Moreover, preventing the proton transfer could greatly increase the free energy barriers for the methylation. Indeed, as shown in Figure 6A and B, preventing the proton transfer (by the SHAKE algorithm in CHARMM²⁷) increases the energy barrier for the 7mX methylation by 3.7 kcal/mol and for the Tb methylation by 12.7 kcal/mol, respectively.

By comparing the two free energy profiles of methylation of 7mX in Figure 6A, it is interesting to note that the profile with the proton fixed overlaps with the profile without fixing the proton until the two profiles approaches transition state (i.e., around $R = 0.17$ Å). Without the proton transfer, the transition state of methylation is much lagged behind and is reached at around $R = 0.64$ Å. This is consistent with the fact that the average structure of each window in Figure 3 before transition

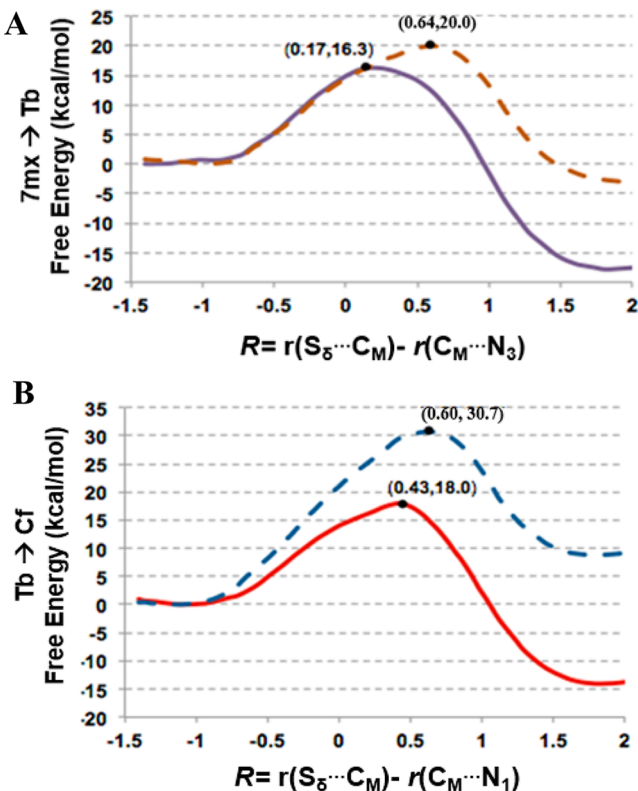


Figure 6. Free energy profiles of methyl transfer to N3 ($7mX \rightarrow Tb$, A) and to N1 ($Tb \rightarrow Cf$, B) of the purine ring. The reaction coordinate: $R = r(C_M \cdots S_\delta) - r(C_M \cdots N_3)$ for methylation of N3 and $R = r(C_M \cdots S_\delta) - r(C_M \cdots N_1)$ for methylation of N1. The solid line shows the energy profile without O-H bond fixed; the dotted line shows the energy profile of simulation with O-H fixed. The free energy barrier near the transition state for each reaction is shown as the second number in the parentheses along with the value of the reaction coordinate (the first number).

state is quite similar to the corresponding one in Figure S2 (see the Supporting Information). By contrast, the free energy profile of methyl transfer to N1 (Figure 6B) shows that preventing the proton transfer increases the free energy change at the beginning of methylation of Tb already. The free energy difference is also reflected in Figure S3 (see the Supporting Information). It appears that the inability of the formation of a stable hydrogen bonding between NE2 of His160 and the fixed proton of Tb may be responsible for the large increase of the free energy barrier. In summary, the results of the simulations seem to suggest that His160 is likely to act as the general acid/base catalyst and mediate the proton transfer for the methylation of N3 and N1. It should be pointed out that the stepwise bond-breaking and -making events might not be well-reflected in the one-dimensional (1D) free energy simulation, and therefore, two-dimensional (2D) simulation involving both methylation and proton transfer might offer a clearer picture on those events.

The 2D free-energy contour map with reaction coordinates for both methylation ($R_x = r(S_\delta \cdots C_M) - r(C_M \cdots N_3)$) and proton transfer ($R_y = r(H \cdots NE2)$) is shown in Figure 7. As demonstrated in Figure 7, the progress of the proton transfer seems to be ahead of the methylation process. Indeed, the proton transfer is basically completed at around the transition state of N3 methylation (point B in Figure 7). The completion

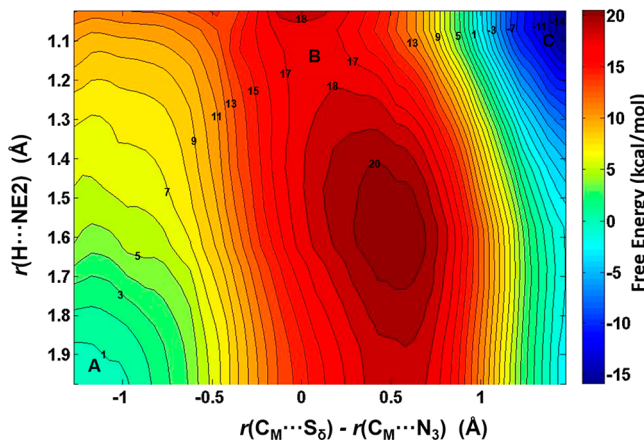


Figure 7. 2D free-energy contour map for N3 methylation of $7mX$. The horizontal axis represents the reaction coordinate of methyl transfer and the vertical axis represents the proton transfer. Points A, B, and C designate the reactant, near transition state, and product complexes, respectively. Some contour lines are shown with respective energy value. The energy bar is shown on the right.

of proton transfer could thereafter promote the final attachment of the positive charged methyl group to the substrate.

The major pathway for caffeine synthesis is thought by a step-by-step methylation of N3 ($7mX \rightarrow Tb$) and then N1 ($Tb \rightarrow Cf$).⁸ Uefuji et al. also detected the activity of DXMT toward paraxanthine (Px).⁸ Px is an isomer of Tb which has two methyl groups on N1 and N7 of its purine ring (Figure 1), while Tb has two methyl groups on N3 and N7. The enzymatic activity of DXMT toward Px is about 10 times higher than that toward Tb.⁸ The MD simulations of the step-by-step methylation was carried out for N1 ($7mX \rightarrow Px$) and then N3 ($Px \rightarrow Cf$). The free energy profiles for the methyl transfer from AdoMet to $7mX$ and Px are plotted in Figure 8, respectively, as a function of the reaction coordinate. The free energy barrier for the N1 methylation on $7mX$ is 17.4 kcal/mol (Figure 8A), which is 1.1 kcal/mol higher than that of N3 methylation on $7mX$. This difference might suggest that DMXT prefer to methylate N3 other than N1 of $7mX$. And this agrees with the experimental fact that the formation of Px from $7mX$ is not detectable.³⁵ Furthermore, the free energy barrier for the conversion of Px to Cf is estimated to be 15.8 kcal/mol (Figure 8B), which is 2.2 kcal/mol lower than that for the conversion of Tb to Cf. DXMT is thus estimated to be much more efficient for converting paraxanthine to caffeine than for converting theobromine to caffeine. This is consistent with the experimental result that the conversion efficiency of Tb to Cf is only 3.8% of that of Px to Cf by DXMT from *Coffee arabica*.⁸ Since the formation of Tb seems to be favored by DXMT compared to Px and the conversion of Px to Cf is much more efficient compared to the conversion of Tb to Px, it might explain why theobromine has been detected in coffee and tea plants, while paraxanthine is rarely detected in the same species.

CONCLUSIONS

In this study, a histidine residue, His160, in the active site of DXMT was identified by the QM/MM MD and free energy simulations as a general base/acid catalyst that accepts the proton from the hydroxyl group of both 7-methylxanthine and theobromine. The computational simulations provided a clearer picture for the catalytic mechanism of DXMT catalyzed methyltransfer process.

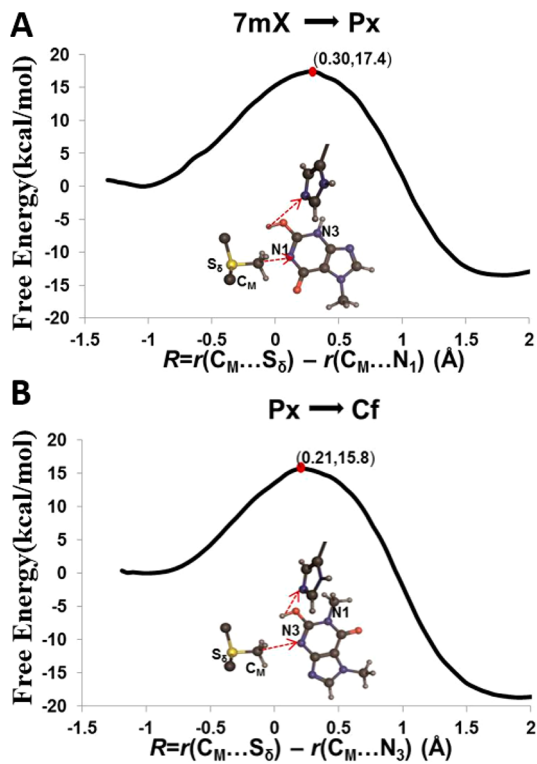


Figure 8. Free energy profiles of methylation through paraxanthine as an intermediate. The N₁ methylation occurs during the conversion of 7mX to Px (A), followed by N₃ methylation for the conversion of Px to Cf (B).

ASSOCIATED CONTENT

Supporting Information

Figure S1, S2, and S3. This material is available free of charge via the Internet at <http://pubs.acs.org>.

AUTHOR INFORMATION

Corresponding Author

*E-mail: hguo1@utk.edu.

Notes

The authors declare no competing financial interest.

ACKNOWLEDGMENTS

We thank Professor Martin Karplus for a gift of the CHARMM program. This work was supported by the National Science Foundation (Grant 0817940 to H.G.). We are also grateful for the computer resources (Newton) from University of Tennessee, Knoxville.

REFERENCES

- (1) Ashihara, H.; Sano, H.; Crozier, A. Caffeine and related purine alkaloids: Biosynthesis, catabolism, function and genetic engineering. *Phytochemistry* **2008**, *69*, 841–856.
- (2) Uefuji, H.; Tatsumi, Y.; Morimoto, M.; Kaothien-Nakayama, P.; Ogita, S.; Sano, H. Caffeine production in tobacco plants by simultaneous expression of three coffee N-methyltransferases and its potential as a pest repellent. *Plant Mol. Biol.* **2005**, *59*, 221–227.
- (3) Waller, G. Biochemical frontiers of allelopathy. *Biol. Plant.* **1989**, *31*, 418–447.
- (4) Kato, M.; Mizuno, K.; Crozier, A.; Fujimura, T.; Ashihara, H. Caffeine synthase gene from tea leaves. *Nature* **2000**, *406*, 956–957.

(5) Ogawa, M.; Herai, Y.; Koizumi, N.; Kusano, T.; Sano, H. 7-Methylxanthine Methyltransferase of Coffee Plants. *J. Biol. Chem.* **2001**, *276*, 8213–8218.

(6) Mizuno, K.; Kato, M.; Irino, F.; Yoneyama, N.; Fujimura, T.; Ashihara, H. The first committed step reaction of caffeine biosynthesis: 7-methylxanthosine synthase is closely homologous to caffeine synthases in coffee (*Coffea arabica* L.). *FEBS Lett.* **2003**, *547*, 56–60.

(7) Mizuno, K.; Okuda, A.; Kato, M.; Yoneyama, N.; Tanaka, H.; Ashihara, H.; Fujimura, T. Isolation of a new dual-functional caffeine synthase gene encoding an enzyme for the conversion of 7-methylxanthine to caffeine from coffee (*Coffea arabica* L.). *FEBS Lett.* **2003**, *534*, 75–81.

(8) Uefuji, H.; Ogita, S.; Yamaguchi, Y.; Koizumi, N.; Sano, H. Molecular Cloning and Functional Characterization of Three Distinct N-Methyltransferases Involved in the Caffeine Biosynthetic Pathway in Coffee Plants. *Plant Physiol.* **2003**, *132*, 372–380.

(9) Yoneyama, N.; Morimoto, H.; Ye, C. X.; Ashihara, H.; Mizuno, K.; Kato, M. Substrate specificity of N-methyltransferase involved in purine alkaloids synthesis is dependent upon one amino acid residue of the enzyme. *Mol. Genet. Genomics* **2006**, *275*, 125–135.

(10) Kato, M.; Mizuno, K. Caffeine synthase and related methyltransferases in plants. *Front. Biosci.* **2004**, *9*, 1833–1842.

(11) McCarthy, A.; McCarthy, J. The Structure of Two N-Methyltransferases from the Caffeine Biosynthetic Pathway. *Plant Physiol.* **2007**, *144*, 879–889.

(12) Mizuno, K.; Kurosawa, S.; Yoshizawa, Y.; Kato, M. Essential region for 3-N methylation in N-methyltransferases involved in caffeine biosynthesis. *Z. Naturforsch. C* **2010**, *65*, 257–265.

(13) Zubietta, C.; Ross, J. R.; Koscheski, P.; Yang, Y.; Pichersky, E.; Noel, J. Structural Basis for Substrate Recognition in the Salicylic Acid Carboxyl Methyltransferase Family. *Plant Cell* **2003**, *15*, 1704–1716.

(14) Yao, J.; Xu, Q.; Chen, F.; Guo, H. QM/MM Free Energy Simulations of Salicylic Acid Methyltransferase: Effects of Stabilization of TS-like Structures on Substrate Specificity. *J. Phys. Chem. B* **2011**, *115*, 389–396.

(15) Guo, H.; Guo, H. Mechanism of histone methylation catalyzed by protein lysine methyltransferase SET7/9 and origin of product specificity. *Proc. Natl. Acad. Sci. U.S.A.* **2007**, *104*, 8797–8802.

(16) Xu, Q.; Chu, Y. Z.; Guo, H. B.; Smith, J. C.; Guo, H. Energy Triplets for Writing Epigenetic Marks: Insights from QM/MM Free-Energy Simulations of Protein Lysine Methyltransferases. *Chem.—Eur. J.* **2009**, *15*, 12596–12599.

(17) Chu, Y.; Xu, Q.; Guo, H. Understanding Energetic Origins of Product Specificity of SET8 from QM/MM Free Energy Simulations: What Causes the Stop of Methyl Addition during Histone Lysine Methylation? *J. Chem. Theory Comput.* **2010**, *6*, 1380–1389.

(18) Brooks, B. R.; Brucoleri, R. E.; Olafson, B. D.; States, D. J.; Swaminathan, S.; Karplus, M. CHARMM: A program for macromolecular energy, minimization, and dynamics calculations. *J. Comput. Chem.* **1983**, *4*, 187–217.

(19) Jorgensen, W.; Chandrasekhar, J.; Madura, J.; Impey, R.; Klein, M. Comparison of simple potential functions for simulating liquid water. *J. Chem. Phys.* **1983**, *79*, 926–935.

(20) Brooks, C. L.; Brunger, A.; Karplus, M. Active site dynamics in protein molecules: a stochastic boundary molecular-dynamics approach. *Biopolymers* **1985**, *24*, 843–865.

(21) MacKerell, A. D.; Bashford, D.; Bellott, M.; Dunbrack, R. L.; Evanseck, J. D.; Field, M. J.; Fischer, S.; Gao, J.; Guo, H.; Ha, S.; Joseph-McCarthy, D.; Kuchnir, L.; Kuczera, K.; Lau, F. T. K.; Mattos, C.; Michnick, S.; Ngo, T.; Nguyen, D. T.; Prodhom, B.; Reiher, W. E.; Roux, B.; Schlenkrich, M.; Smith, J. C.; Stote, R.; Straub, J.; Watanabe, M.; Wiorkiewicz-Kuczera, J.; Yin, D.; Karplus, M. All-atom empirical potential for molecular modeling and dynamics studies of proteins. *J. Phys. Chem. B* **1998**, *102*, 3586–3616.

(22) Elstner, M.; Porezag, D.; Jungnickel, G.; Elsner, J.; Haugk, M.; Frauenheim, T.; Suhai, S.; Seifert, G. Self-consistent-charge density-functional tight-binding method for simulations of complex materials properties. *Phys. Rev. B* **1998**, *58*, 7260–7268.

- (23) Cui, Q.; Elstner, M.; Kaxiras, E.; Frauenheim, T.; Karplus, M. A QM/MM Implementation of the Self-Consistent Charge Density Functional Tight Binding (SCC-DFTB) Method. *J. Phys. Chem. B* **2001**, *105*, 569–585.
- (24) Field, M. J.; Bash, P. A.; Karplus, M. A combined quantum mechanical and molecular mechanical potential for molecular dynamics simulations. *J. Comput. Chem.* **1990**, *11*, 700–733.
- (25) Torrie, G. M.; Valleau, J. P. Monte-Carlo free energy estimates using non-Boltzmann sampling. Application to the subcritical Lennard-Jones fluid. *Chem. Phys. Lett.* **1974**, *28*, 578–581.
- (26) Kumar, S.; Bouzida, D.; Swendsen, R. H.; Kollman, P. A.; Rosenberg, J. M. The weighted histogram analysis method for free-energy calculations on biomolecules. I. The method. *J. Comput. Chem.* **1992**, *13*, 1011–1021.
- (27) Ryckaert, J.; Ciccotti, G.; Berendsen, H. Numerical integration of the Cartesian equation of motion of a system with constraints: molecular dynamics of n-alkanes. *J. Comput. Phys.* **1977**, *23*, 327–341.
- (28) Callahan, M. P.; Gengeliczki, Z.; Svadlenak, N.; Valdes, H.; Hobza, P.; de Vries, M. S. Non-standard base pairing and stacked structures in methyl xanthine clusters. *Phys. Chem. Chem. Phys.* **2008**, *10*, 2819–2816.
- (29) Rostkowski, M.; Olsson, M.; Søndergaard, C. R.; Jensen, J. H. Graphical analysis of pH-dependent properties of proteins predicted using PROPKA. *BMC Struct. Biol.* **2011**, *11*, 6.
- (30) Anandakrishnan, R.; Aguilar, B.; Onufriev, A. H++ 3.0: automating pK prediction and the preparation of biomolecular structures for atomistic molecular modeling and simulations. *Nucleic Acids Res.* **2012**, *40*, W537–W541.
- (31) Zhang, X.; Bruice, T. C. Catalytic Mechanism and Product Specificity of Rubisco Large Subunit Methyltransferase: QM/MM and MD Investigations. *Biochemistry* **2007**, *45*, 5505–5514.
- (32) Hu, P.; Wang, S.; Zhang, Y. How Do SET-Domain Protein Lysine Methyltransferases Achieve the Methylation State Specificity? Revisited by Ab Initio QM/MM Molecular Dynamics Simulations. *J. Am. Chem. Soc.* **2008**, *130*, 3806–3813.
- (33) Yao, J.; Chu, Y.; An, R.; Guo, H. Understanding Product Specificity of Protein Lysine Methyltransferases from QM/MM Molecular Dynamics and Free Energy Simulations: The Effects of Mutation on SET7/9 beyond the Tyr/Phe Switch. *J. Chem. Inf. Model.* **2012**, *52*, 449–456.
- (34) Chu, Y.; Li, G.; Guo, H. QM/MM MD and free energy simulations of the methylation reactions catalyzed by protein arginine methyltransferase PRMT3. *Can. J. Chem.* **2013**, *91*, 605–612.
- (35) Roberts, M. F.; Waller, G. R. N-methyltransferases and 7-methyl-N-nucleoside hydrolase activity in Coffea arabica and the biosynthesis of caffeine. *Phytochemistry* **1979**, *18*, 451–455.